

# Predicting a third planet in the Kepler-47 circumbinary system

Tobias C. Hinse

*Korea Astronomy & Space Science Institute, Republic of Korea*

*Armagh Observatory, College Hill, BT61 9DG, Northern Ireland, UK*

tchinse@gmail.com

Nader Haghighipour

*Institute for Astronomy, University of Hawaii-Manoa, Honolulu, Hawaii, USA*

Veselin B. Kostov

*Johns Hopkins University, Baltimore, USA*

Krzysztof Goździewski

*Toruń Centre for Astronomy of the Nicolai Copernicus University, Grudziadzka 5, Poland*

## ABSTRACT

We have studied the possibility that a third circumbinary planet in the Kepler-47 planetary system be the source of the single unexplained transiting event reported during the discovery of these planets. We applied the MEGNO technique to identify regions in the phase space where a third planet can maintain quasi-periodic orbits, and assessed the long-term stability of the three-planet system by integrating the entire 5 bodies (binary + planets) for 10 Myr. We identified several stable regions between the two known planets as well as a region beyond the orbit of Kepler-47c where the orbit of the third planet could be stable. To constrain the orbit of this planet, we used the measured duration of the unexplained transit event ( $\sim 4.15$  hours) and compared that with the transit duration of the third planet in an ensemble of stable orbits. To remove the degeneracy among the orbits with similar transit durations, we considered the planet to be in a circular orbit and calculated its period analytically. The latter places an upper limit of 424 days on the orbital period of the third planet. Our analysis suggests that if the unexplained transit event detected during the discovery of the Kepler-47 circumbinary system is due to a planetary object, this planet will be in a low eccentricity orbit with a semimajor axis smaller than 1.24 AU. Further constraining of the mass and orbital elements of this planet requires a re-analysis of the entire currently available data including those obtained post-announcement of the discovery of this system. We present details of our methodology and discuss the implication of the results.

*Subject headings:* circumbinary planets, stability, celestial mechanics

## 1. Introduction

During the past few years, *Kepler* telescope has discovered several planets in circumbinary orbits. All these planets have been detected photometrically, exhibiting transit signatures when passing in front of the stars of the binary. The first of these circumbinary planets (CBPs) was Kepler-16b discovered by Doyle et al in 2011. Since then several more *Kepler* CBPs have been discovered, namely Kepler-38b (Orosz et al. 2012a), Kepler-34b and Kepler-35b (Welsh et al. 2012), Kepler-47b&c (Orosz et al. 2012b), Kepler-64b (Kostov et al. 2013; Schwamb et al. 2013), Kepler-413b (KIC 12351927b) (Kostov et al. 2014), and KIC 9632895b (Welsh et al. 2014).

Among the currently known *Kepler* circumbinary planetary systems, Kepler-47 presents an interesting case. The fact that this system harbors two planets is a strong indication that similar to planet formation around single stars, circumbinary planets can also form in multiples. The latter implies that more planets may exist in any of the currently known circumbinary systems. In the Kepler-47 system, the existence of a third planet was speculated in its 2012 discovery paper as a way to account for an unexplained feature observed in the light curve of this binary (Orosz et al. 2012b). As reported by these authors, a single, 0.2% deep transit event had been detected which could not be explained by the two known transiting planets.

In this paper, we plan to test the above-mentioned hypothesis. Our approach is to study the dynamics of the three-planet system, and use long-term stability to identify the viable regions where the orbit of the third planet would be stable. Using dynamical stability to predict additional planets has been presented in several other studies (Barnes & Raymond 2004; Raymond & Barnes 2005; Fang & Margot 2012). In cases where stable regions are identified, we will use transit timing and transit duration variations to constrain the orbit of the third planet.

The dynamics and orbital stability of planets in circumbinary orbits have been the subject of studies for close to three decades. Dvorak (1986), Rabl & Dvorak (1988), and Holman & Wiegert (1999) carried out long-term orbital integrations of test-particles aiming at exploring a large area of the system's parameter space. In particular, for P-type orbits, the authors established stability criteria for a planet's semimajor axis as a function of the binary orbital parameters and mass-ratio. Musielak et al. (2005) and Eberle et al. (2008) also studied the stability of planetary orbits in P-type systems and presented criteria for stable, marginally stable, and unstable circular planetary orbits. Recent analytic analysis of the dynamics of circumbinary planets has also been presented by Doolin & Blundell (2011), and Leung & Lee (2013).

This paper is structured as follows. In section 2, we briefly review the Kepler-47 system

as described by Orosz et al. (2012b). In section 3, we describe our numerical techniques and in section 4, we present the results of our stability analysis using the chaos indicator MEGNO (Mean Exponential Growth factor of Nearby Orbits). In section 5, we calculate the transit durations of Kepler-47b and the candidate third planet, and compare them with their measured value as reported by Orosz et al. (2012b) to constrain the orbit of the third planet. Finally, in section 6, we conclude this study by presenting a summary and discussing the implications of the results.

## 2. The Kepler-47 system

Kepler-47 is a single-lined spectroscopic binary with a  $1.043 M_{\odot}$  primary and a secondary with a mass of  $0.362 M_{\odot}$ . The period of this binary is 7.5 days. In 2012, Orosz et al. announced the detection of two planets in circumbinary orbits around this system. These authors analyzed long- and short-cadence photometric data from *Kepler* space telescope, spanning 1050.5 days from Quarter 1 to 12, and identified eighteen transit events of the inner planet (Kepler-47b) and three for the outer planet (Kepler-47c). Table 1 shows the published (osculating) orbital parameters of Kepler-47 and its two planets. We note that because of observational degeneracies, not all orbital parameters can be determined from the photodynamical<sup>1</sup> model as described in Orosz et al. (2012b). We also note that all orbital elements are in the (geometric) Jacobian coordinate system.

The inner planet, Kepler-47b, with a period of 50 days, is the smaller of the two with a radius of  $\sim 3$  Earth-radii. Orosz et al. (2012b) estimated that the mass of this planet is 7-10 Earth-masses. Due to the non-detection of ETVs, an upper limit of 2 Jupiter-masses can firmly be established for this object. The outer planet, Kepler-47c, has an orbital period of  $\sim 303$  days with a  $\sim 4.6$  Earth-radii. The authors estimated a plausible mass in the range 16-23 Earth-masses. The upper limit for the mass of this planet was determined to be 28 Jupiter-masses.

In their analysis of the light curve of Kepler-47 system, Orosz et al. (2012b) detected a single transit event that could not be explained by the transits of the two planets. With a formal significance of  $10.5\sigma$ , this transit event occurred at BJD  $2,455,977.363 \pm 0.004$ , approximately 12 hours after the last transit of Kepler-47b in the Q12 data set. The duration of this transit was observed to be  $\sim 4.15$  hours. Orosz et al. (2012b) suggested that if this transit event is due to a third planet, given its depth of 0.2%, the planet must have a radius  $\simeq 4.5$  Earth-radii.

The rest of this paper is devoted to examining this hypothesis using dynamical considerations. Integrating the five-body system of the binary and three planets, we will determine the ranges of the parameters for which the orbit of a hypothetical third planet will be stable, and using the properties

---

<sup>1</sup><https://github.com/dfm/photodynam>

of the above-mentioned single transit event, we will identify the most probable regions around the binary where the orbit of this planet may exist.

### 3. Methodology and Numerical Techniques

We note that results presented in this work have been obtained from direct numerical integration of the equations of motion using the initial conditions shown in Table 1. The orbit of the binary system is fully resolved and the three planets are treated as massless as well as massive objects.

We adopted two different algorithms for solving equations of motion: The IDL implementation of the Livermore Solver (LSODE) which is an adaptive algorithm with a step-size control, and an accurate extrapolation method implemented as the Gragg-Bulirsch-Stoer (GBS) algorithm (the ODEX code) (Hairer, Norsett & Wanner 1993). The latter is frequently used in celestial mechanics and orbit calculations (see Goździewski et al. 2012; Goździewski et al. 2013; Goździewski & Migaszewski 2014, and references therein). **Both algorithms use a relative and absolute error tolerance parameter to control the integration accuracy. We set these parameters to one part in  $10^{15}$ . When integrating several test orbits of the five-body problem, we obtained identical results using both algorithms.**

**We would like to note that, when transforming orbital elements, we use Jacobi-like coordinates with a mass-parameter  $\mu = k^2(M_1 + M_2 + m_i)$  for each planet. Here  $m_i$  is the mass of the  $i$ th planet,  $M_1$  and  $M_2$  represent the masses of the binary stars, and  $k$  is the Gauss gravitational constant. The transformed orbital elements are then given relative to the center of mass of the binary system. This approach differs from the usual definition of Jacobi elements where the position and velocity of a planet are given relative to the center of mass of all remaining massive bodies within its orbit.**

Our stability analysis employs the well-established fast chaos indicator MEGNO technique (Cincotta & Simó 1999, 2000; Cincotta, Giordano & Simó 2003) which enables us to explore the phase space topology of the system. The MEGNO technique has found widespread applications within dynamical astronomy (Goździewski et al. 2001; Goździewski 2003; Goździewski et al. 2008; Hinse et al. 2010; Kostov et al. 2013) and is closely related to the Fast Lyapunov Indicator (FLI) (Mestre et al. 2011). In brief, MEGNO, shown by  $\langle Y \rangle$  here and throughout the paper, has the following properties. For initial conditions resulting in quasi-periodic orbits,  $\langle Y \rangle \rightarrow 2.0$  for  $t \rightarrow \infty$ . For chaotic orbits,  $\langle Y \rangle \simeq 2\lambda/t$  for  $t \rightarrow \infty$  where  $\lambda$  is the Maximum Lyapunov Exponent (MLE). In the simulations presented in this paper, we chose to stop a given integration when  $\langle Y \rangle > 5$ . Orbits with quasi-periodic time evolution usually assume values of  $|\langle Y \rangle - 2| < 0.001$  at the end of the

numerical integration. We used the MEGNO implementation within the MECHANIC package (Stonina et al. 2015), and considered the integration time for each orbit to be  $4.7 \times 10^4$  binary periods.

#### 4. Orbital stability of the third planet

We begin our stability analysis by adding a hypothetical third planet (hereafter shown by letter d) to the Kepler-47 system. Our goal is to identify regions of the parameter space where the third planet can have a long-term stable orbit. Throughout our analysis, we start planets Kepler-47b and c at their published osculating elements (Table 1) and set their masses equal to 10 and 23 Earth-masses, respectively. The initial orbital orientation of the third planet is taken to be co-aligned with Kepler-47c.

We first consider the third planet to be massless. Figure 1 shows the values of MEGNO for different initial values of the semimajor axis and eccentricity of the third planet in an  $(a, e)$  space. The initial osculating elements for the two known planets are shown by black dots. The color-coding in this and subsequent MEGNO maps represents the value of MEGNO,  $\langle Y \rangle$ . Higher values (lighter colors) correspond to higher degree of chaos and therefore, higher chance of instability. As shown here, there are **three** regions where a third planet can maintain a quasi-periodic orbit: **i) a region in the vicinity of Kepler-47b**, **ii) a region between the two known planets**, and **iii) the region exterior to the orbit of Kepler-47c** (but interior to the general quasi-periodic area shown in dark colors).

**In a multi-planet system, different types of perturbation affect the dynamical evolution of the system on different timescales. In general, there is a timescale associated with the effect of short-term MMRs, a timescale due to secular resonances (slow variation of orbital elements), and a longer evolutionary timescale due to the tidal effects, mass-loss and other weak perturbations. When using a fast stability indicators such as MEGNO, because the properties of a given solution in the phase-space must be determined on a small length of the orbit, the stability of a particular orbital configuration must be presented in the context of these timescales. In a compact configuration, for instance when the third planet is between Kepler-47b and c, the dynamics of the system is mainly affected by the short-term 2-body and 3-body MMRs. Similar numerical experiments such as those by Goździewski & Migaszewski (2014) and references therein suggest that in a study as the one presented in this paper, when the value of MEGNO converges to 2 (indicating a quasi-periodic orbit), the stability of the system (the orbit-crossing time) is guaranteed for a time 2–3 orders of magnitude longer than the MEGNO integration time-span. In the case of the Kepler-47 system, the crossing-time is longer than at least  $\sim 5 \times 10^7$  binary period. The protecting effect of MMRs imply that in**

some regions such as a number of orbits in the islands of quasi-periodicity at  $a_d < 1.5$  AU (figure 1), the entire five-body system will be stable for even longer times (e.g., as long as the lifetime of the system’s stars).

It is important to note that when longer-period, multi-body mean-motion or secular resonances exist, the convergence of MEGNO for relatively short integration times does not necessarily imply stability for the lifetime of the binary. The perturbations from these resonances may result in dynamical instability over tens of millions or billions of years (e.g., Laskar & Gastineau 2009). That means that either the MEGNO integrations must cover a significant fraction of the secular timescales, or direct numerical integrations have to be carried out in order to ensure that the system is stable over the time-span of interest.

Despite the above-mentioned shortcoming, MEGNO integrations can still provide accurate and reliable characterization of the phase-space with a very small CPU overhead. They are also very useful in obtaining rough stability limits. In figure 1, we have plotted such limits (black curves) around the orbit-crossing curves of the third planet with Kepler-47b and c (red curves) following the semi-empirical stability criterion presented by Giuppone, Morais & Correia (2013). The stability criterion by these authors has been derived from the Wisdom’s stability criterion for the restricted three-body problem. Unfortunately, this criterion does not seem to determine the limits of stable regions in the Kepler-47 system, properly. For instance, as it will be shown later, the interesting region of  $0.5(\text{AU}) \leq a_d \leq 1.5(\text{AU})$  is considered to be unstable when using the stability criterion by Giuppone, Morais & Correia (2013). However, as our MEGNO maps show (see also figure 2), this region contains a set of MMRs where the entire five-body system can be stable. A similar argument applies to the region immediately beyond the orbit of Kepler-47c. As indicated by our calculations, a few islands of stability exist in this area that correspond to two-body MMRs (e.g., 3d:4c, 2d:3c and 4d:7c), whereas according to the stability criterion by Giuppone, Morais & Correia (2013), this region is unstable.

In figure 2, we show these regions in more detail. In each panel, we label each quasi-periodic island with its associated two-body mean-motion resonance. Tables 2 and 3 give the values of the inner and outer semimajor axis of the third planet indicating the width of each resonance valid for the third planet on a circular orbit.

From all the orbits shown in figure 2, we chose 11 (labelled as IC1 to IC11 standing for Initial Conditions 1 to 11) and studied their long-term dynamical evolution by integrating them for  $10^7$  years. Results for initial conditions IC1 and IC2 are shown in figure 3. In order to highlight the details of the evolution of these orbits, we only show the results of the first 10,000 years of integrations. As shown here, both orbits have identical initial eccentricities (0.01). However, their initial semimajor axes are different by  $\Delta a = 0.0127$  AU. Results indicated that despite such a

small difference in initial conditions, the evolutions of these two orbits are profoundly different. A chaotic characteristics is clearly visible for IC2 which exhibits a random walk in semimajor axis and eccentricity. This random walk is an indication of a stochastic process over time, slowly destabilizing the orbit by driving the orbital eccentricity to unity. We find the third planet to be eventually ejected from the system after some 190,000 yrs. For IC1, the third planet follows a bound stable quasi-periodic orbit over at least  $10^7$  years and shows no sign of chaotic diffusion. The orbital evolution of the two known planets of the system, Kepler-47b and Kepler-47c (both with their assigned masses) show similar dynamical behavior with their orbits bound between a minimum and maximum value for their orbital elements.

#### 4.1. Identification of two-body resonances

In figure 2, we have labelled the islands of quasi-periodic orbits with their associated mean-motion resonances. To illustrate the true resonant character of these orbits, we have calculated their critical arguments (resonant angle) using

$$\theta_{md:lc} = l\lambda_c - m\lambda_d - n\varpi_c - p\varpi_d. \quad (1)$$

In this equation,  $\lambda$  and  $\varpi$  denote the mean longitude and longitude of pericenter, respectively and coefficients  $(l, m, n, p)$  are integer numbers satisfying d’Alambert rule. We found that the resonant angle corresponding to each quasi-periodic island exhibits a clear librational behavior around zero degrees. We show the time evolution of the resonant angle for a few selected initial conditions (IC1, IC3, IC4 in the region between Kepler-47b and c, and IC8 beyond the orbit of Kepler-47c) in figure 4. As shown in this figure, the variation of the resonance angle for IC8 has larger amplitudes. The MMR-locking is deep in all cases and supports the interpretation that the islands of quasi-periodic orbits in the MEGNO dynamical maps are associated with mean-motion resonances. This results also has encouraging implications for the possible detection of a third planet since MMRs can lead to an amplified TTV signals compared to those of the orbits in non-resonant configurations (Agol et al. 2005, 2007; Haghighipour & Kirste 2011).

#### 4.2. Predicting the Mass of the third planet

Results shown in the previous section enabled us to identify regions of the parameter space where a test particle could maintain a stable orbit alongside the two massive planets, Kepler-47b and c. In reality, however, the third planet is also massive and its interaction with other planets

can alter the orbital architecture of the system. In the following, we will explore the dynamical characteristics of the system by considering the third planet to be massive as well.

As stated by Orosz et al. (2012b), the mass of the putative third planet is practically unconstrained. However, the depth of its single transit points towards a planet with a radius of  $\simeq 5$  Earth-radii. Because of the lack of a precise model for the density and interior of such planets, we consider a range of values for the mass of the third planet from 0 to 150 Earth-masses.

Figures 5 and 6 show the results of the calculation of MEGNO for the entire 5-body system considering the third planet to have a mass of 0, 10, 23 and 100 Earth-masses. We probed the semimajor axis of the third planet in the interval of 0.1 AU to 1 AU in figure 5 and between 1 AU and 3 AU in figure 6. In all maps, we considered the orbital eccentricity of the third planet to vary in the range of 0 to 0.5. As shown in these figures, there are regions between planets Kepler-47b and c where the third planet can have stable orbits. These figures also show the change in the mass of the third planet does not seem to have a significant impact on the overall dynamical structure of the system. However, subtle differences do appear. For instance, a close inspection of the results indicates that the quasi-periodic regions around Kepler-47b tend to diminish with increasing the mass of the third planet. Also, considering a massless third planet at a semimajor axis of 0.989 AU with an eccentricity of 0.15 seems to result in a chaotic orbit. However, increasing the mass of the planet to 100 Earth-masses renders the orbit with the same initial condition, quasi-periodic.

We also noticed that some of the mean-motion resonances around 0.8 AU had vanished when considering the third planet to be of 100 Earth-masses. For such a high value of the mass, the locations of quasi-periodic mean-motion resonances between the third planet and Kepler-47c appear to have shifted to smaller semimajor axes. The effect of changing the values of the mass of a planet on the location of mean-motion resonances has been illustrated in detail by Goździewski et al. (2013) in their study of the system of  $\nu$  Octantis. In general, resonances may become wider/narrower or even split if the masses of planets change. Diminished quasi-periodic regions exterior to the orbit of Kepler-47c were also observed when the third planet was taken to be 100 Earth-masses. It seems that low-eccentricity, co-orbital, quasi-periodic orbits are more likely when the third planet has a higher mass.

Results shown in figures 5 and 6 suggest that a third planet in a low-eccentricity orbit can be stable in the region between Kepler-47b and c, and also for semimajor axes larger than 1.75 AU. The main requirement for long-term orbital stability is set by the third planet’s pericenter distance. In order for the planet to be stable, this distance has to be well-separated from Kepler-47b and c (hence its low-eccentricity orbit) so that the gravitational perturbation of these bodies cannot alter the dynamics of the planet.

To examine the long-term stability of the third planet, we carried out two single-orbit inte-



grations for  $10^7$  years. We considered the third planet to be 50 Earth-masses and chose its initial semimajor axis and eccentricity the same as in IC3 in figure 2 (the third planet being interior to Kepler-47c) and IC6 in figure 2 (the third planet being exterior to Kepler-47c). Figure 7 shows the result. As shown here, no sign of chaotic diffusion is observed for any values of the orbital elements of the third planet. This suggests that a third planet with a mass of 30 Earth-masses or smaller can have a stable orbit either between the two known planets (IC3) or in an orbit exterior to Kepler-47c (IC6). The orbits of planets b and c exhibit a very weak signature of chaotic dynamics. In both simulations, the orbits of these planets remained bound and did not show any sign of a random walk.

We carried out similar simulations for higher values of the mass of the third planet. We found that the simulation with initial conditions IC3 results in chaotic and unstable orbits when the mass of the third planet is as high as 150 Earth-masses. However, when starting the third planet with initial conditions IC6, we found that larger masses are allowed rendering an overall stable configuration.

## 5. Analysis of transit timing and transit duration variations

As shown in the previous section, dynamical considerations point to regions in the Kepler-47 two-planet system where a third body can have a stable orbit. However, this orbit is unconstrained. In this section, we use the measured time and duration of transits in the Kepler-47 system to constrain the orbit of the third planet.

We start by calculating transit duration (TDV) and transit timing variations (TTV) induced by the third planet on Kepler-47b. Due to its shorter orbital period, this planet has higher number of transits providing a large set of measurements for comparison and verification purposes.

To calculate the values of TTV and TDV of a planet, we use the same numerical integration algorithm that was used in generating MEGNO maps. We integrate the full five-body system using the values of the masses and radii of the stars and planets as well as the orbital elements of the two known planets as given in Table 1. During the integration, we monitor the on-sky projected position of the planet ( $r_{\text{sky}}$ ) relative to the primary star. Once the planet has crosses the north-south axis passing through the center of the star, we determine the time of ingress ( $t_1$ ) from a series of back- and forth-integrations. At each integration step, the quantity  $r_{\text{sky}}$  is compared to the sum of the star and planet radii  $R_A + R_{\text{pl}}$ . In each iteration, our algorithm decreases the time step by a third in order to ensure convergence. The time of ingress is defined when  $r_{\text{sky}} - (R_A + R_{\text{pl}}) < 10^{-15}$ . From reversing the velocities of all bodies, the egress time  $t_2$  is determined. The mid-transit time is then calculated from  $t_1 + (t_2 - t_1)/2$ . We use linear regression to calculate the variations in the

transit times (TTV). The transit duration (TDV) is calculated using  $(t_2 - t_1)$ . We have tested the calculation of TTV by reproducing the results given in Nesvorný & Morbidelli (2008).

Figure 8 shows the results for Kepler-47b. We considered the third planet to have 1 Earth-mass and started it at the initial condition IC6. The top three panels in figure 8 show the resulted variations in the semimajor axis, eccentricity, and inclination. The bottom two panels show the values of the TTV and TDV. Here we have connected consecutive transit events with a solid line. The vertical lines show the cycle numbers for which the first or last transit is detected while being part of a consecutive transit series. An example of a consecutive transit series is the transits 59 to 105. As shown in the bottom two panels, there are two gaps between transits 22 and 59, and between transits 105 and 143 (where there is missing data). In these gaps, isolated timing measurements (shown by plus signs) represent non-consecutive transit events. In other words, for those TTV/TDV data points that are not connected, the planet did not transit the star before and after the given data point. For instance, we see from figure 8 that there are four isolated near-miss transits after the transit cycle 22. There are missing transits in all gaps which have not been plotted for the obvious reason. Such missed transit events were also observed in the light curve of Kepler-413b (Kostov et al. 2014). The only explanation for such single-transit or near-miss events is the short-term variations in the planets orbital elements. As shown in figure 8, the orbital elements of Kepler-47b do indeed undergo significant changes from one transit to another suggesting that the gaps are due to the low orbital inclination of Kepler-47b relative to the plane of the sky. We recall that the closer the inclination is to  $90^\circ$ , the closer the planet will be transiting along the star’s equator. Therefore, for the specific geometry of the Kepler-47 system, the projected orbital plane of Kepler-47b on the plane of the sky will be outside the star’s disk ( $r_{\text{sky}} - R_{\text{pl}} > R_A$ ) and therefore, no timing measurements can be computed. As a result, such events do not appear in figure 8. However, for a given value of the orbital inclination, we do obtain single transit events and alternating missing transits when Kepler-47b is close to the edge of the star.

Interestingly, we see no near-miss or isolated transit prior to transit 59. A detailed examination of the light curve at around transit 59 shows that the transit-to-transit variations in semimajor axis and eccentricity of Kepler-47b are minimal. We conclude that the short-term orbital variations are significant and capable of shifting the planet’s projected disk in and out of the stellar disk. This is an interesting result as missing transit events can be used to further constrain the results of photodynamical models in future discoveries of transiting circumbinary planets.

### 5.1. Transit duration of the third planet

In this section, we calculate the durations of the transits of the third planet and compare them with the duration of the single, unexplained transit event of the system to constrain the orbit of this

body. It is important to note that because of the mutual interactions between planets, the duration of the transits of the third planet will vary from one transit cycle to another. Figure 9 shows this for different values of mass and initial orbital configuration of the third planet. In making this figure, we only considered initial conditions for which our MEGNO calculations indicated quasi-periodic orbits. In particular, we considered initial conditions IC1 to IC11 shown in figure 2 (except for IC2 for which the orbit of the planet was found to be highly chaotic). We also considered two cases for the mass of the third planet: A mass-less object shown on the left panels, and a 10 Earth-mass planet depicted on the right. The methodology for calculating transit duration is similar to the procedure described in the previous section. In each panel, the horizontal line at 4.15 hours corresponds to the duration of the single transit event identified by Orosz et al. (2012b). As shown in figure 9, in general, the mass of the planet does not play a significant role in the duration of its transit. We found that in spite of its variations, there are several transit cycles in which the duration of the transit of the third planet is comparable to that of the observed single transit ( $\sim 4.15$  hours). For instance, in the top-left panel of figure 9 where the planet is mass-less and starts at the initial condition IC1, the transit number 83 appeared to have a duration of 4.16 hours. Transit durations of around 4 hours were also found for initial conditions IC3 and IC4. We recall that IC1, IC3 and IC4 are initial conditions where the third planet starts between the two planets Kepler-47b and c. We also found that when the planet is massive, transit durations of around 4 hours are possible for the initial condition IC6 where the orbit of the third planet is exterior to Kepler-47c.

The results mentioned above point to a strong degeneracy. It seems impossible to determine the correct orbit of the third planet using its transit duration. This degeneracy can, however, be broken assuming the third planet is in a circular orbit. As shown by Kostov et al. (2013), in this case, the orbital period of the third planet can be determine using

$$P_d = P_{\text{bin}}(0.74\sqrt{1 - b^2} + 0.26)^{-3}, \quad (2)$$

where  $b$  is the (a priori unknown) impact parameter. As  $b$  varies only between 0 and 1, we can use equation (1) to constrain the orbital period of the third planet and break the degeneracy. Specifically, if  $b = 0$  (i.e. a central transit) then  $P_d = P_{\text{bin}}$ , representing a third body with the same orbit as that of the binary. This is consistent with the measured transit duration of 4.15 hours being comparable to the duration of the stellar eclipse. On the contrary, if  $b \approx 1$  (i.e. a grazing transit), equation (1) gives  $P_d = 57 \times P_{\text{bin}}$ , suggesting an upper limit for the period of the third planet of  $\sim 424$  days. For a binary mass of  $1.4M_{\odot}$  this corresponds to a semimajor axis of  $\sim 1.24$  AU, effectively ruling out initial conditions IC6 through IC11, as well as orbits with progressively larger semimajor axis. Thus the third planet is either on a stable orbit in the vicinity of Kepler-47b or between the two known planets Kepler-47b and c, or started along IC5.

## 6. Discussion & Conclusions

In this study, we used dynamical considerations to examine the possibility that the single, unexplained transit in the Kepler-47 system as reported by Orosz et al. (2012b) would be due to a third planet. Using the MEGNO technique, we identified regions in the phase-space where the third planet could follow quasi-periodic orbits considering the five-body problem. We determined several of such quasi-periodic regions between the two known planets Kepler-47b and Kepler-47c, where they also include orbital mean-motion resonances with either one of the two bodies.

Using accurate single orbit integrations, we examined the long-term orbital stability of the third planet within the framework of a five-body problem. Results identified ranges of semimajor axis and eccentricity that would render the third planet stable over a time period of 10 million years. To examine the extent of the dependence of the results on the mass of this planet, we carried out integrations for different values of its mass, and showed that a third planet with a mass as high as 50 Earth-masses can still maintain stable orbits either between Kepler-47b and Kepler-47c, or beyond the orbit of Kepler-47c. For higher masses of the third planet the quasi-periodic stable regions in the vicinity of Kepler-47b ceases. For a selection of initial conditions within quasi-periodic islands we established a clear association of these islands with two-body mean-motion resonances by demonstrating a librating (around zero) critical argument.

To constrain the orbit of the third planet, we calculated its transit durations as well as the TTV and TDV of Kepler-47b for various initial conditions. We found that transit duration and transit timing variations are affected by short-term changes in the orbit that have been caused by perturbations due to other bodies in the system. This implies that it is imperative to consider gravitational interactions when studying multi-body systems where mutual perturbations can be significant.

**Also, when the line-of-sight inclination of the transiting planet becomes small (planet approaches the limb of the star), short-term perturbation on timescales on the order of the orbital period will have the effect of shifting the on-sky position of the planet. This can result in missing transits from one orbit to the other. These transit-missing events can be used to further constrain best-fit photodynamical models. In this study, for the first time, we have correlated the cause of missing transits with the short-term (transit-to-transit) variations of orbital elements. We also confirmed the possibility of long-duration transits. For instance in figure 9, considering the case of IC6 for a mass-less third planet, the duration of a single transit can last for nearly 60 hours.**

When calculating transit durations of the third planet, we found that the results suffer from a large degeneracy. Several orbits produced similar transit durations as that of the single transit, 4.15 hours. We were able to break this degeneracy for circular orbits and determined an upper limit of

424 days for the orbit of the third planet.

**In a recent study by Kratter & Shannon (2014), a period of 186 days was conjectured for the third planet in Kepler-47. Using Kepler’s third law, we obtain a semi-major axis of 0.714 AU (relative to the binary center of mass) for the third planet, placing it close to the stable 5c:8d mean-motion resonance or nearby resonances (see figure 2) with Kepler-47c. Our work predicts several islands of quasi-periodic orbits in the neighbourhood of the 186 days orbit. Kratter & Shannon (2014) also carried out long-term numerical integrations of the five-body system. Their results support the finding that all planets maintain stable orbits over at least  $2 \times 10^6$  years.**

In the present analysis we suggest that a third planet could in fact be the cause of the single, unexplained transit event reported by Orosz et al. (2012b). This planet will have a low eccentricity orbit either i) in the vicinity of Kepler-47b (for low masses), ii) between planets Kepler-47b and Kepler-47c, or iii) exterior to planet c with a semimajor axis smaller than 1.24 AU.

**The detection of a third planet could follow along the route of measuring TTVs or TDVs of Kepler-47b and/or Kepler-47c as caused by this planet. However, the process of finding additional bodies using timing variations is highly degenerate and can lead to various dynamical configurations that produce the same timing signal (Nesvorný 2009; Nesvorný & Beaugé 2010). We therefore suggest that the entire currently available Kepler photometric data on Kepler-47 to be analyzed and searched for additional transit signatures that can not be explained by the two known planets Kepler-47b and Kepler-47c.**

TCH acknowledges support from the Korea Astronomy and Space Science Institute (KASI) grants 2012-1-410-02 and 2014-1-400-06, and the Korea Research Council for Fundamental Science and Technology (KRCF). Calculations were carried out at the SFI/HEA Irish Center for High-End Computing (ICHEC) and the KMTNet computing cluster in South Korea. Research at the Armagh Observatory is funded by the Department of Culture, Arts & Leisure (DCAL). TCH would like to thank the Institute for Astronomy and the NASA Astrobiology Institute at the University of Hawaii for their warm hospitality during a visit in Nov/Dec 2012 when part of this work was carried out. TCH would also like to thank David Nesvorný for fruitful discussion on calculating TTV and TDV. NH acknowledges support from NASA ADAP grant NNX13AF20G, NASA Origins grant NNX12AQ62G, HST grant HST-GO-12548.06-A, and Alexander von Humboldt Foundation. Support for program HST-GO-12548.06-A was provided by NASA through a grant from the Space Telescope Science Institute, which is operated by the Association of Universities for Research in Astronomy, Incorporated, under NASA contract NAS5-26555. VBK gratefully acknowledges support from NESSF grant NNX13AM33H. This work has been supported by Polish National Science Centre MAESTRO grant DEC 2012/06/A/ST9/00276 (K.G.). The authors would

like to thank to anonymous referee for valuable suggestions.

## REFERENCES

- Agol, E., Steffen, J., Saari, R. & Clarkson, W., 2005, MNRAS, 359, 567
- Agol, E. & Steffen, J. H., 2007, MNRAS, 374, 941
- Barnes, R., Raymond, S. N., 2004, ApJ, 617, 569
- Cincotta, P. M. & Simó, C., 1999, CeMDA, 73, 195
- Cincotta, P. M. & Simó, C., 2000, A & AS, 147, 205
- Cincotta, P. M., Giordano, C. M., Simó, C., 2003, Physica D: Nonlinear Phenomena, 182, 151
- Doolin, S., Blundell, K. M., MNRAS, 2011, 418, 2656
- Doyle L. R., Carter J. A., Fabrycky D. C., Slawson R. W., Howell S. B., et al. 2011, Science, 333, 1602
- Dvorak R., 1986, A&A, 167, 379
- Eberle, J., Cuntz, M., Musielak, Z. E., 2008, IAUS, 249, 507
- Fang J., Margot J.-L., 2012, ApJ, 751, 23
- Giuppone, C. A., Morais, M. H. M., Correia, A. C. M., 2013, MNRAS, 436, 3547
- Goździewski, K., Bois, E., Maciejewski, A. J., Kiseleva-Eggleton, L., 2001, A&A, 378, 569
- Goździewski, K., 2003, A&A, 398, 315
- Goździewski, K., Breiter, S., Borczyk, W., 2008, MNRAS, 383, 989
- Goździewski, K. et al., 2012, MNRAS, 425, 930
- Goździewski K., Słonina M., Migaszewski C., Rozenkiewicz A., 2013, MNRAS, 430, 533
- Goździewski K. & Migaszewski C., 2014, MNRAS, 440, 3140
- Book: "Planets in Binary Star Systems" Haghighipour, N., 2010, Astrophysics and Space Science Library, Volume 366. ISBN 978-90-481-8686-0
- Haghighipour, N., & KIRSTE, S., 2011, Celest. Mech. Dynamic. Astronom., 111, 267
- Hairer E., Norsett S. P., Wanner G., Solving Ordinary Differential Equations I. Berlin: Springer-Verlag; 1993. Non-stiff Problems.

- Holman, M. J. & Wiegert, P. A., 1999, *AJ*, 117, 621
- Hinse, T. C., Christou, A. A., Alvarellos, J. L. A., Goździewski, K., 2010, *MNRAS*, 404, 837
- Kostov V. B., McCullough P. R., Hinse T. C., Tsvetanov Z. I., Hébrard G., et al. 2013, *ApJ*, 770, 52
- Kostov V. B., McCullough P. R., Carter J. A., Deleuil M., Díaz R. F., et al. 2014, *ApJ*, 784, 14
- Kratter, K. M., Shannon, A., 2014, *MNRAS*, 437, 3727
- Laskar, J., Gastineau, M., *Nature*, 2009, 459, 817
- Leung, G. C. K., Lee, M. H., *ApJ*, 2013, 763, 107
- Mestre, M. F., Cincotta, P. M., Giordano, C. M., 2011, *MNRAS*, 414, 100
- Musielak, Z. E., Cuntz, M., Marshall, E. A., Stuit, T. D., *A&A*, 2005, 434, 355
- Nesvorný, D., Morbidelli, A., 2008, *ApJ*, 688, 636
- Nesvorný, D., 2009, *ApJ*, 701, 1116
- Nesvorný, D., Beaugé, C., 2010, *ApJ*, 709, 44
- Orosz J. A., Welsh W. F., Carter J. A., Brugamyer E., Buchhave L. A., et al. 2012a, *ApJ*, 758, 87
- Orosz J. A., Welsh W. F., Carter J. A., Fabrycky D. C., Cochran W. D., et al. 2012b, *Science*, 337, 1511
- Rabl G., Dvorak R., 1988, *A&A*, 191, 385
- Raymond, S. N., Barnes, R., 2005, *ApJ*, 619, 549
- Schwamb M. E., Orosz J. A., Welsh W. F., Carter J. A., Fabrycky D. C., et al. 2013, *ApJ*, 768, 127
- Słonina, M., Goździewski, K., Migaszewski, C., 2015, *New Astronomy*, 34, 98-107
- Welsh W. F., Orosz J. A., Carter J. A., Fabrycky D. C., Ford E. B., et al. 2012, *Nature*, 481, 475
- Welsh, W. F., Orosz, J. A., Short, D. R., Haghhighipour, N., et al., 2014, submitted to *ApJ*, (arXiv:1409.1605)



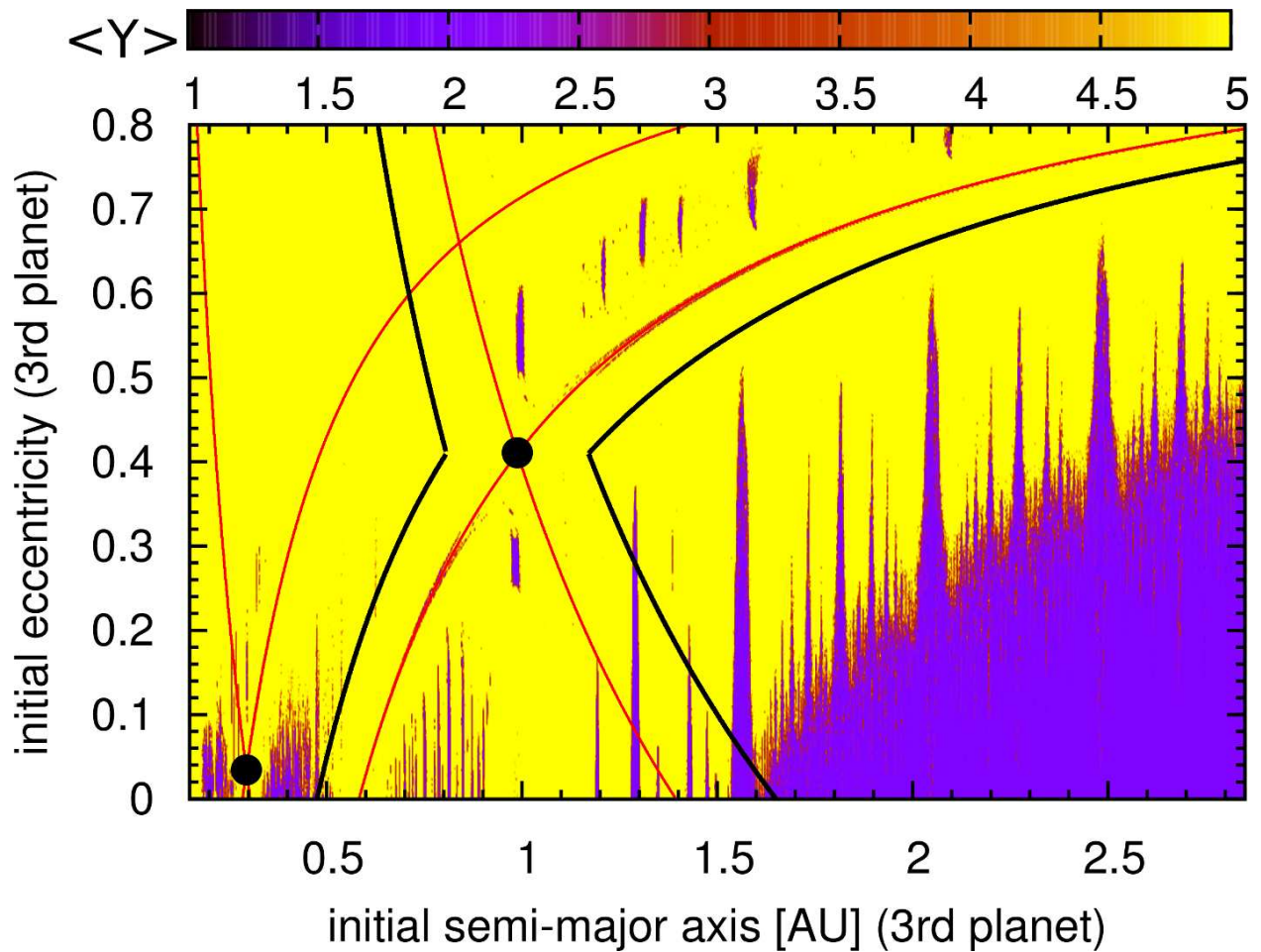


Fig. 1.— Dynamical MEGNO map for the third planet of the Kepler 47 system. The two known planets, Kepler-47b and c are shown as black circles. The vertical and horizontal axes correspond to the initial values of the eccentricity and semimajor axis of the third planet. Yellow color denotes chaotic dynamics and blue indicates quasi-periodic orbits. The general quasi-periodic region for a third planet starts from around 1.6 AU. Several quasi-periodic areas for a third planet are also embedded in the general chaotic regions between the two known planets. Red and black contour lines corresponds to collision (red) and semi-empirical stability criterion (black) (Giuppone, Morais & Correia 2013). See text for more details.

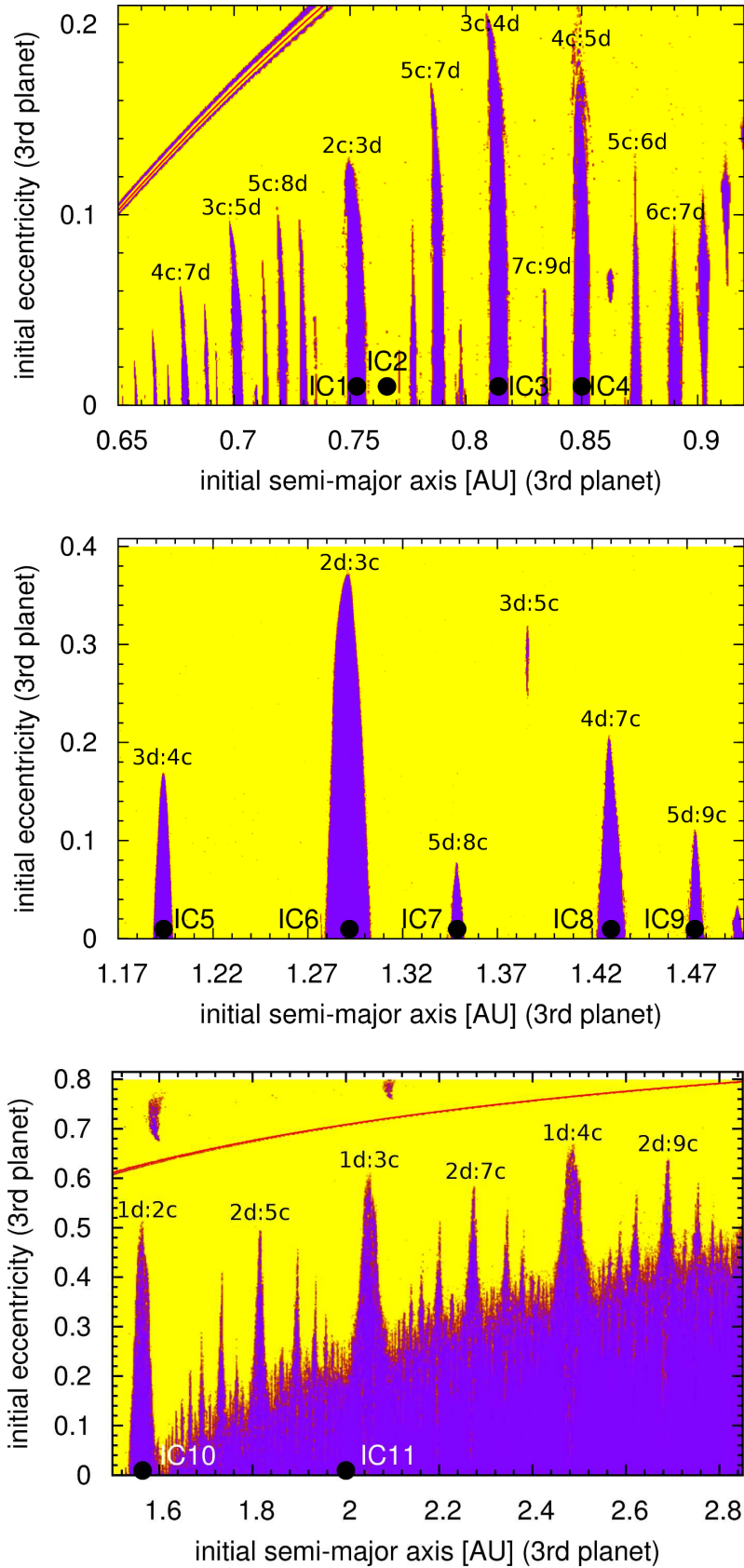


Fig. 2.— Same as figure 1 but zooming into three specific regions. The top panel shows the case where the third planet is between Kepler-47b and c. The bottom two panels correspond to the case where the third planet is outside the orbit of Kepler-47c. The color-coding is the same as that in figure 1.

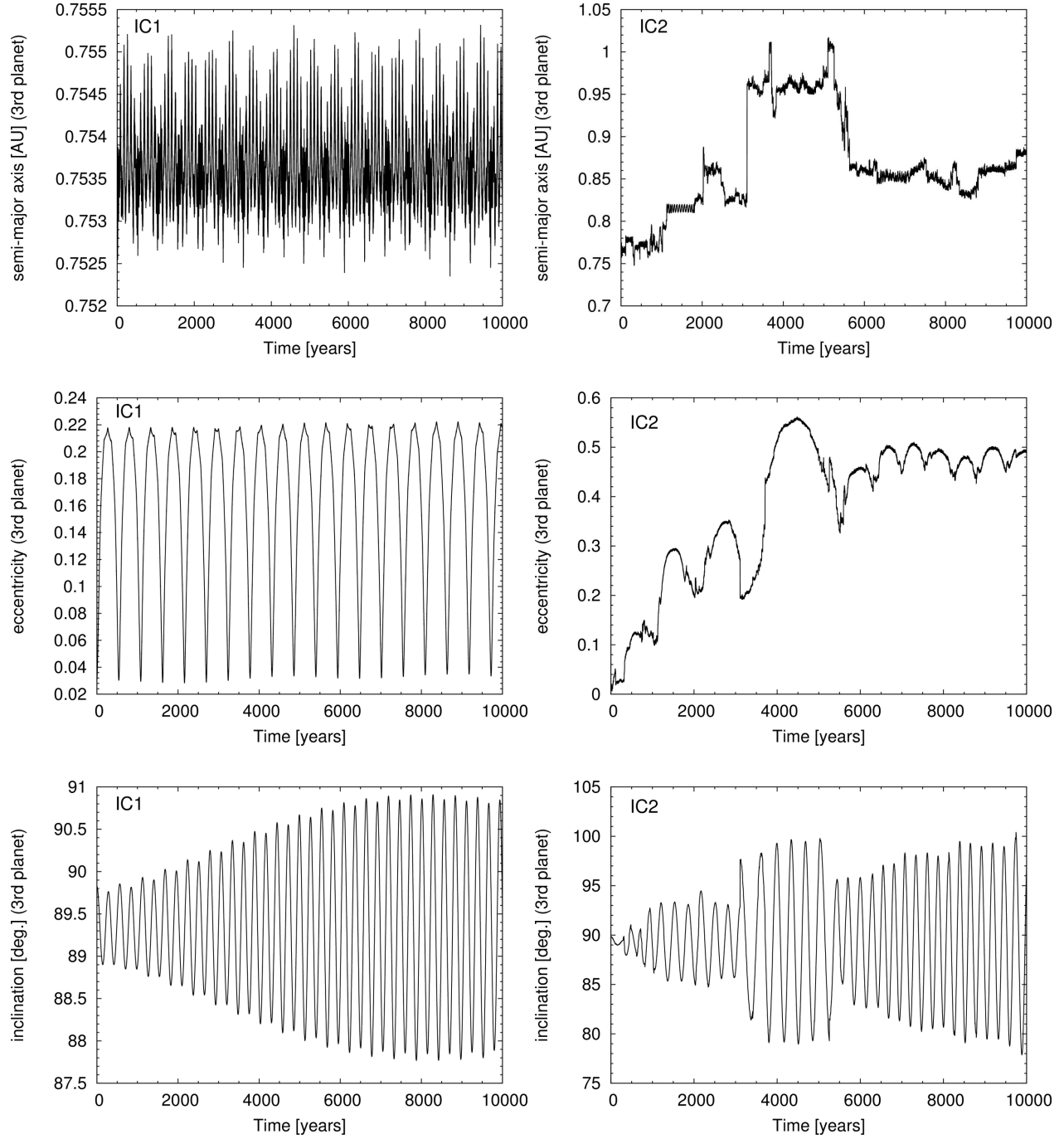


Fig. 3.— Time evolution of (Jacobian) orbital element of a **third massless companion** considering initial conditions IC1 (left) and IC2 (right). Both orbits have initial eccentricity of 0.01. However, for IC2, the initial semimajor axis of the planet is slightly larger at 0.7657 AU.

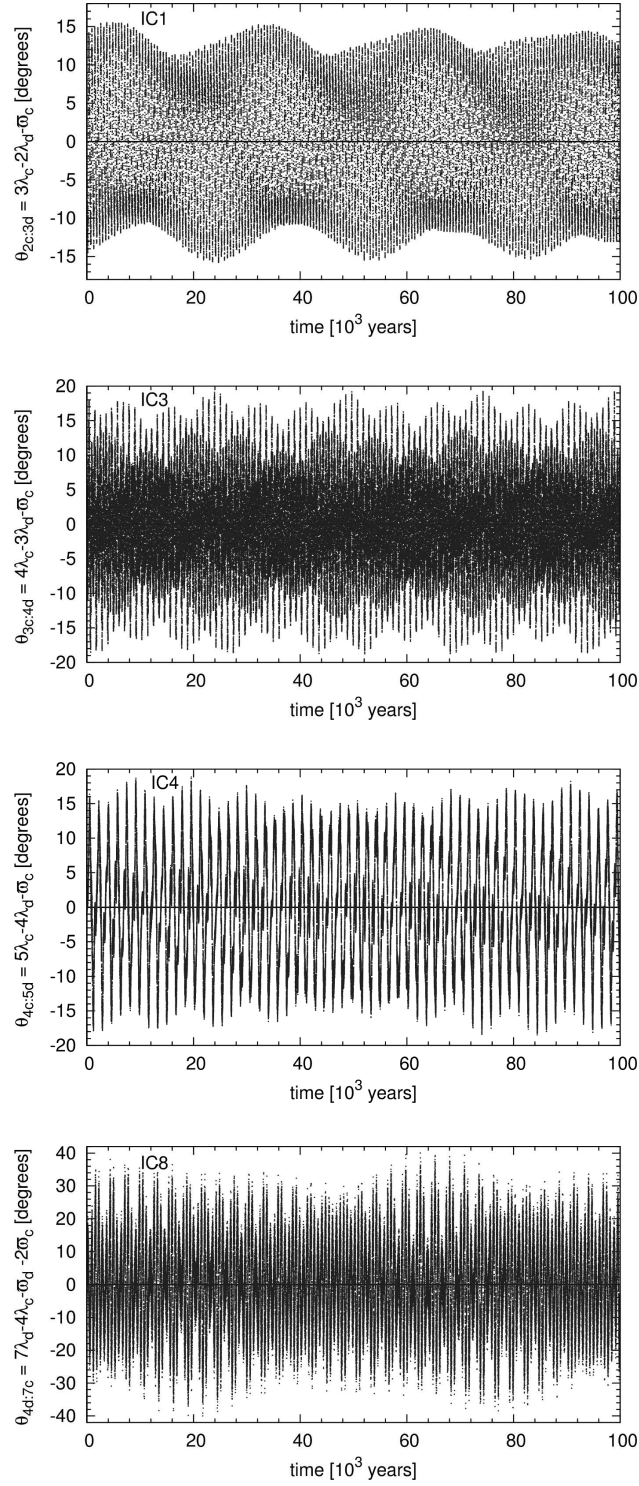


Fig. 4.— Time evolution of the resonant angle ( $\theta$ ) for a selection of initial conditions (IC1, IC3, IC4 and IC8). In all cases we find the resonant argument to librate around zero. This finding supports the results obtained from MEGNO confirming the correct identification of quasi-periodic MMRs in the semi-major axis – eccentricity space of the third planet.

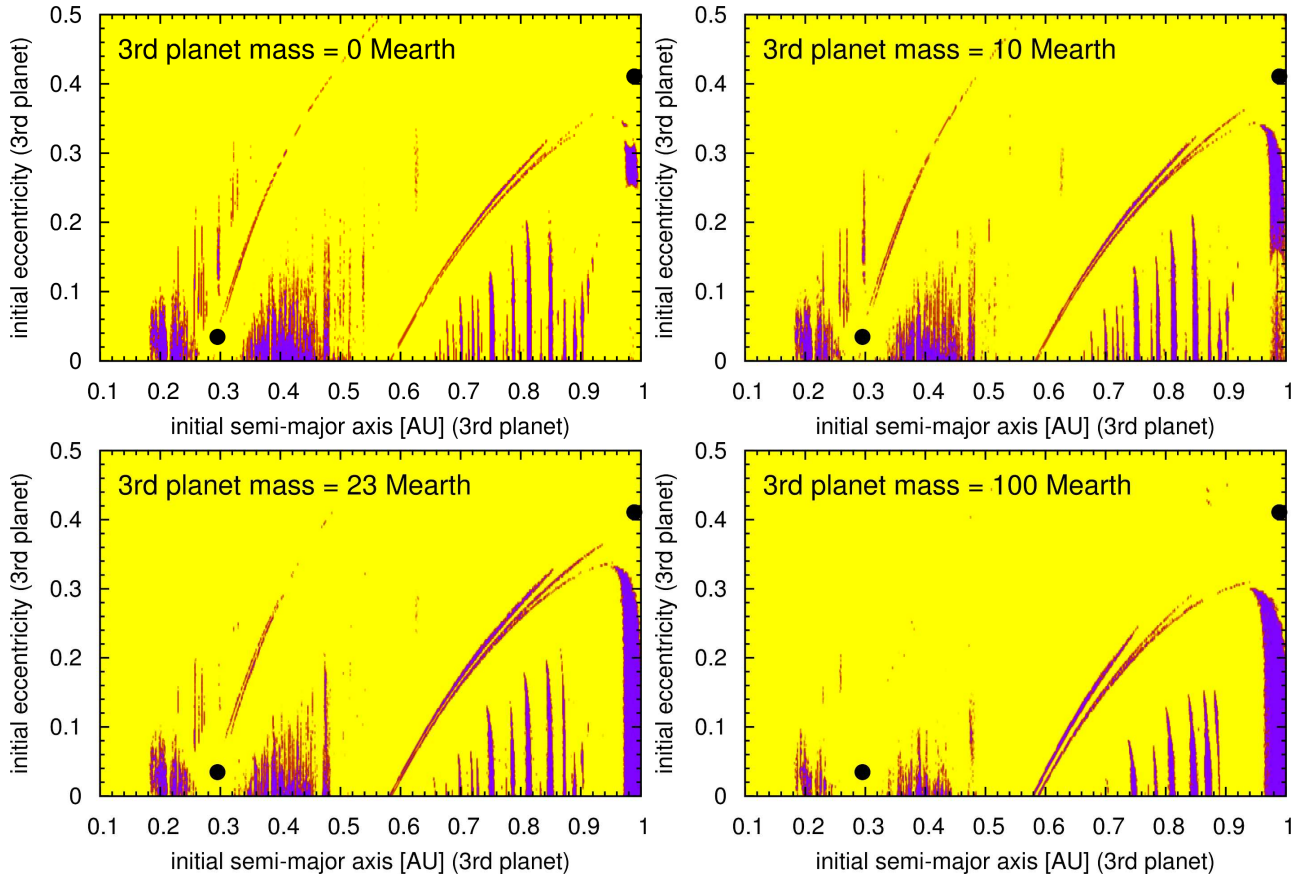


Fig. 5.— Dynamical MEGNO maps of the third planet for different values of its mass. Integrations were carried out considering the full five-body system. The two planets Kepler-47b and c are shown by black circles. Initial orbital elements of these two planets were taken from Table 1. Color coding is the same as in figure 1.

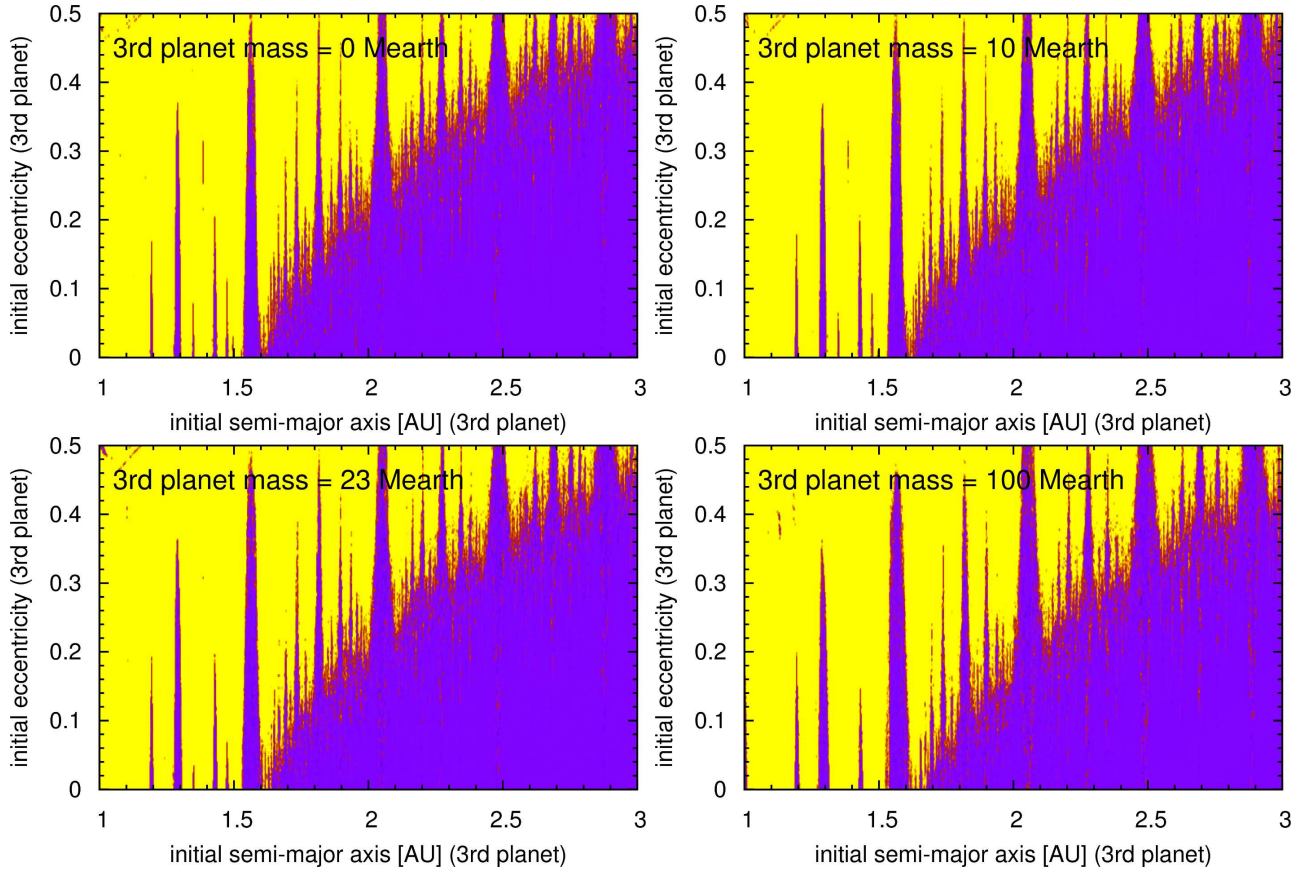


Fig. 6.— Same as figure 5 but probing the region exterior to the orbit of Kepler-47c. Color coding is the same as in figure 1.

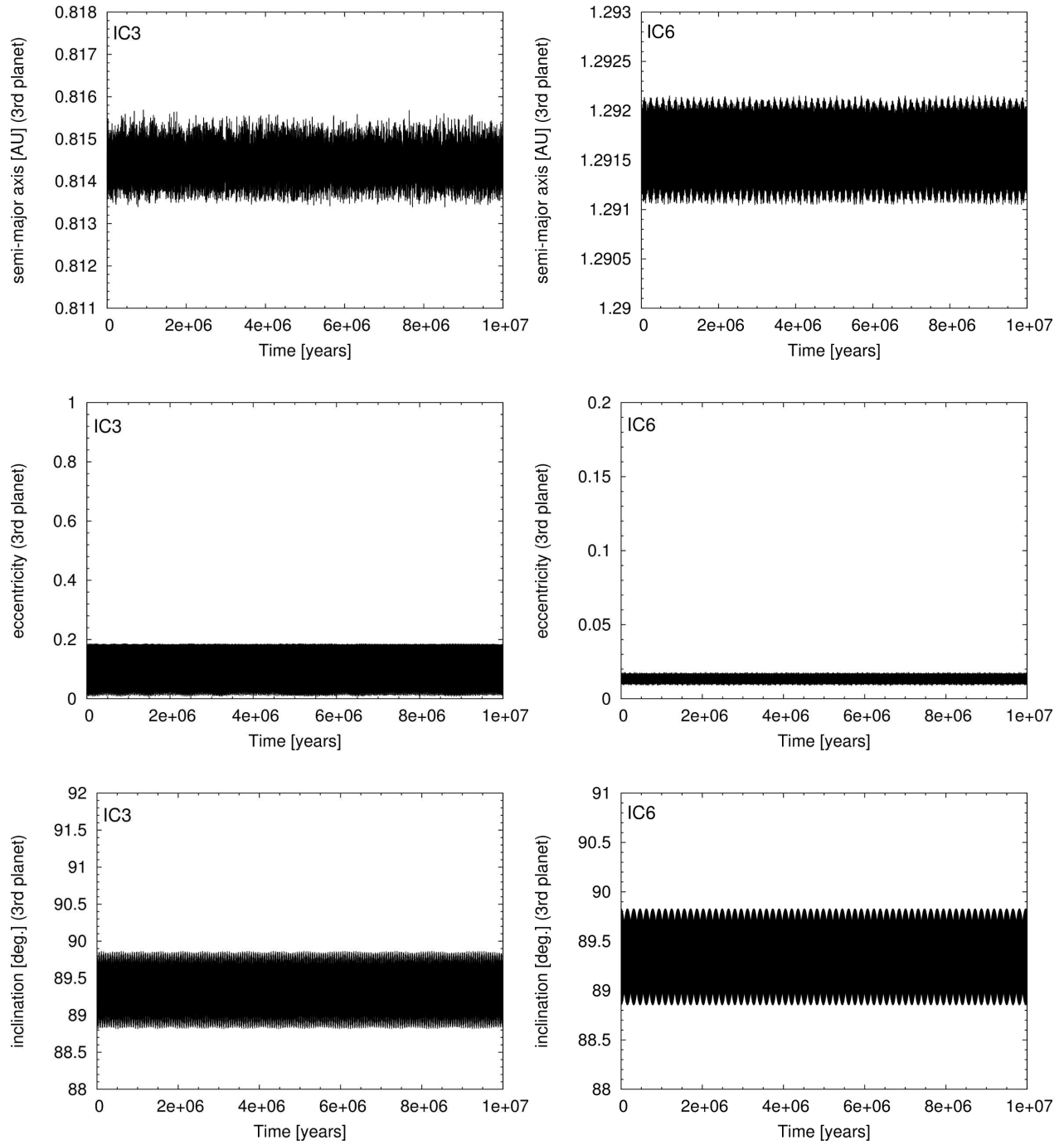


Fig. 7.— Time evolution of (Jacobian) orbital element of the third planet considering initial conditions IC3 (left; third planet between Kepler-47b and c) and IC6 (right; third planet exterior to Kepler-47c). In both cases, the mass of the third planet is 50 Earth-masses.

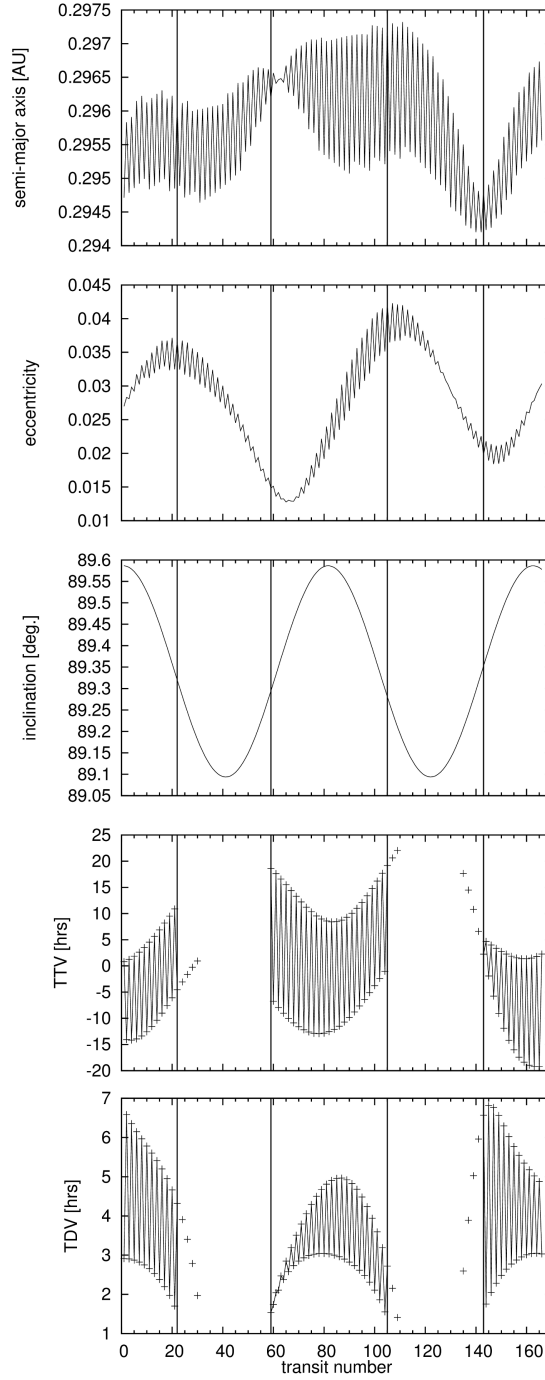


Fig. 8.— Time evolution of the orbital elements of Kepler-47b (top three panels) and graphs of its TTV and TDV (bottom two panels). We considered the third planet to be Earth-massed and started it at initial condition IC6. Vertical lines correspond to transit cycles 22, 59, 105 and 143. We note that the intersection of vertical lines with the inclination curve occur at different orbital inclinations as a consequence of the short-term orbital variations of Kepler-47b. Usually a single critical inclination is determined which corresponds to an impact parameter of one solar radius. The total duration corresponds to  $\simeq 165 \times 49.5$  days = 22.4 years.



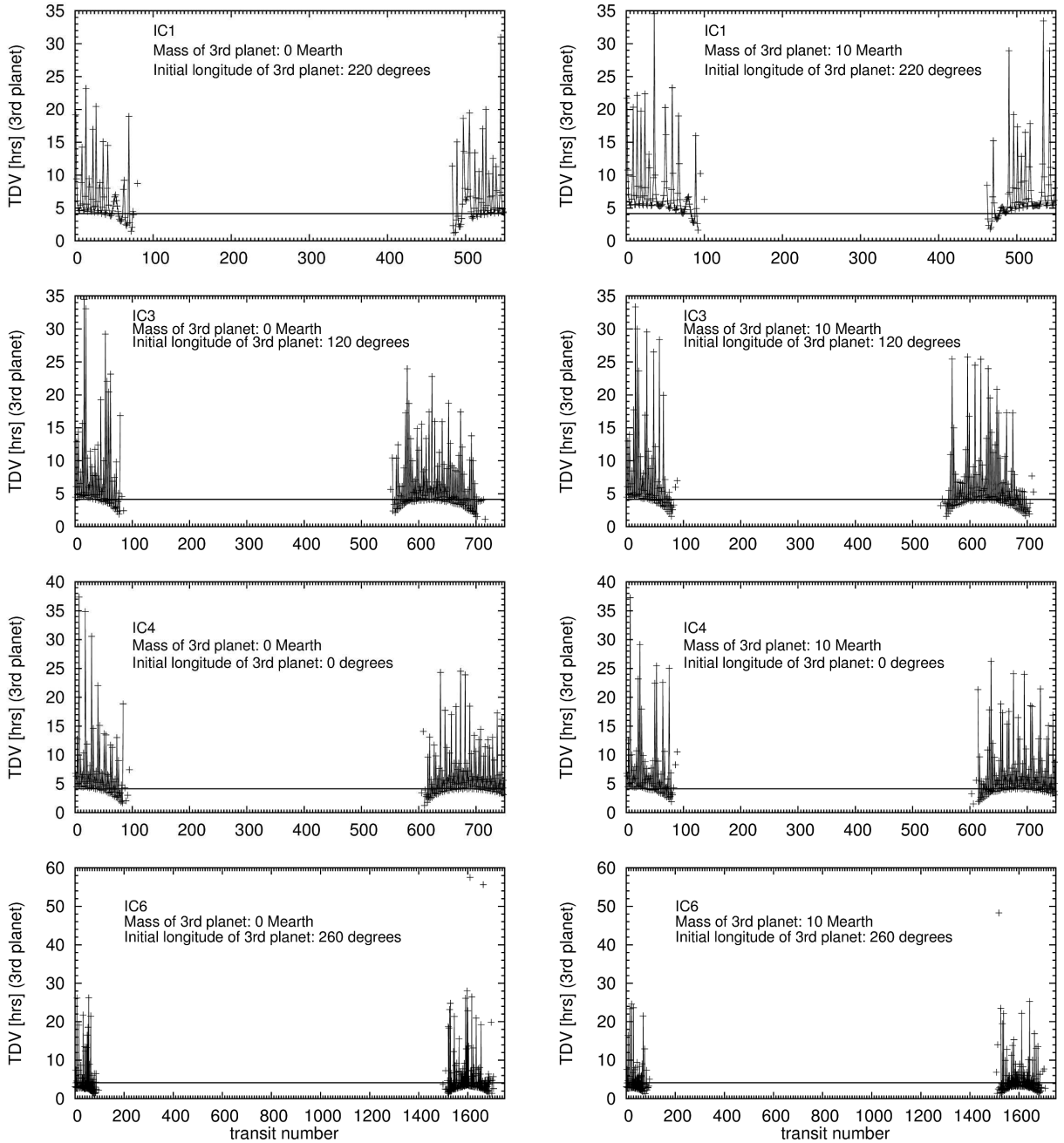


Fig. 9.— Graphs of the transit duration of the third planet for various initial conditions. The left column corresponds to a massless object and the right column is for a 10 Earth-mass planet. The horizontal line marks a transit duration of 4.15 hours. We considered various initial mean longitudes of the third planet. Other initial mean longitudes were also tried and resulted in similar results. As shown here, the duration of the transit does not have strong dependence on the initial phase of the third planet. Also, no significant differences between transit durations of a test mass and a massive planet were observed. Symbols that are not connected with a line have a missed trailing or leading transit, and represent isolated transit events. Note the increase in the period of transit durations for longer periods of the transiting third planet.

Table 1: Orbital parameters of the Kepler-47 system and their  $1\sigma$  uncertainties (Orosz et al. 2012b).

Parameter	Kepler-47 (Star B)	Kepler-47b	Kepler-47c
Semi-major axis (AU)	$0.0836 \pm 0.0014$	$0.2956 \pm 0.0047$	$0.989 \pm 0.016$
Eccentricity	$0.0234 \pm 0.001$	0.034	0.41
Inclination (deg.)	$89.34 \pm 0.12$	$89.59 \pm 0.50$	$89.826 \pm 0.010$
Argument of pericenter (deg.)	$212.3 \pm 4.4$	0.0 (fixed)	0.0 (fixed)
Longitude of node (deg.)	0.0 (fixed)	0.0 (fixed)	0.0 (fixed)
Mean anomaly (deg.)	0.0 (fixed)	0.0 (fixed)	0.0 (fixed)
Orbital period (days)	$\simeq 7.5$	$\simeq 49.5$	$\simeq 303.2$
Mass	$0.362 M_{\odot}$	$10 M_{\oplus}$	$23 M_{\oplus}$
Radius	$0.3506 R_{\odot} \pm 0.0063$	$2.98 R_{\oplus} \pm 0.12$	$4.61 R_{\oplus} \pm 0.20$

---

Note. — **The inclination of the third planet was chosen to be equal to the inclination of Kepler-47c, and the remaining angles were set to zero.** Orbital elements indicated by “(fixed)” have been undetermined from observations. **The mass parameter  $\mu = k^2(M_1 + M_2 + m_i)$  has been used for a given planet with mass  $m_i$  when transforming elements.** Symbols  $R_{\oplus}$  and  $M_{\oplus}$  denote the radius and mass of Earth. **The mass of the primary star (Star A) is  $1.043 M_{\odot}$ .**

Table 2: Mean-motion resonances between Kepler-47c and the third planet (d) when this object is in a circular orbit between planets b and c.

Resonance	$a_{\text{inner}}$ [AU]	$a_{\text{outer}}$ [AU]
4c:7d	0.677	0.680
3c:5d	0.700	0.704
5c:8d	0.720	0.723
2c:3d	0.749	0.757
5c:7d	0.786	0.791
3c:4d	0.811	0.818
7c:9d	0.833	0.835
4c:5d	0.847	0.853
5c:6d	0.871	0.875
6c:7d	0.888	0.893

---

Note. — Quantities  $a_{\text{inner}}$  and  $a_{\text{outer}}$  denote the inner and the outer boundary of the quasi-periodic regions shown in figure 2 for a circular orbit.

Table 3: Same as Table 2 with the exception that the third planet is in an orbit exterior to Kepler-47c.

Resonance	$a_{\text{inner}}$ [AU]	$a_{\text{outer}}$ [AU]
3d:4c	1.189	1.199
2d:3c	1.279	1.303
5d:8c	1.346	1.352
3d:5c	1.385	1.386
4d:7c	1.424	1.437
5d:9c	1.471	1.478
1d:2c	1.538	1.595

---

Note. — Mean-motion resonances with semimajor axes larger than 1.6 AU have not been included.